Brilliant blue, green, yellow, and red fluorescent diamond particles: synthesis, characterization, and multiplex imaging demonstrations

Nunn, N; Prabhakar, Neeraj; Reineck, P; Magidson, V; Kamiya, E; Heinz, WF; Torelli, MD; Rosenholm, Jessica; Zaitsev, A; Shenderova, O

Published in:
Nanoscale

DOI:
10.1039/C9NR02593F

Published: 01/01/2019

Document Version
Submitted manuscript

Document License
CC BY-NC-ND

Brilliant Blue, Green, Yellow, and Red Fluorescent Diamond Particles: Synthesis, Characterization, and Multiplex Imaging Demonstrations

Nicholas Nunn[1*], Neeraj Prabhakar[2], Phillip Reineck[3], Valentin Magidson[4], Erina Kamiya[5], William F. Heinz[4], Marco D. Torelli[1] Jessica Rosenholm[2], Alexander Zaitsev[6], Olga Shenderova[1*]

[1] Adámas Nanotechnologies, Inc. 8100 Brownleigh Drive, Suite 120 Raleigh, NC 27617, USA

[2]Pharmaceutical Sciences Laboratory, Faculty of Science and Engineering, Åbo Akademi University, Tykistokatu 6A, Turku 20520, Finland

[3]ARC Centre of Excellence for Nanoscale BioPhotonics & School of Science, RMIT University, Melbourne, VIC 3001, Australia

[4]Optical Microscopy and Analysis Laboratory, Cancer Research Technology Program, Frederick National Laboratory for Cancer Research, Frederick, MD 21702, USA

[5]Optical Microscopy and Analysis Laboratory, Office of Science and Technology Resources, Center for Cancer Research, National Cancer Institute, National Institutes of Health, Frederick MD 21702, USA

[6]College of Staten Island (CUNY), 2800 Victory Blvd., Staten Island, NY 10312, USA

**Corresponding Authors:*

N. Nunn, nnunn@adamasnano.com;

O. Shenderova, oshenderova@adamasnano.com

Abstract

Until recently, the number of emission colors available from fluorescent diamond particles has been limited to near-infrared fluorescence from the nitrogen-vacancy color center in type Ib synthetic diamond and green fluorescence associated with the nitrogen-vacancy-nitrogen center in type Ia natural diamond. Using our recently reported rapid thermal annealing technique, we demonstrate the capability of producing nanodiamond particles that exhibit distinctive blue, green, yellow, and red fluorescence from the same synthetic diamond starting material. Utilizing these multiple colored diamonds, we analyze their fluorescence characteristics both in solution as well as at a single particle level and

additionally evaluate their viability in simple multiplex imaging and cellular bioimaging experiments. While there are still challenges associated with their immediate use in traditional multiplex imaging, this novel approach opens new opportunities to enhance the capability and flexibility of fluorescent diamond particles at the nanoscale.

1. Introduction

Targeted fluorescent imaging is widely used in biomedical research and is being investigated for translational implementation in clinical applications, with several ongoing clinical trials.[1] Demand exists for fluorescent labels which are non-toxic, bright, photostable, targetable, and possess the capability for multiplex imaging. Targeted labeling coupled with multiplex fluorescence imaging can provide profound insight into complex biological structures and interactions at the cellular and sub-cellular level, allowing the microscopist or biologist the ability to selectively study specific biomarkers amidst an array of surrounding components simultaneously, ideally without *a priori* knowledge of the spatial arrangement of the biological moieties under study.[2-6] However, it is rare that traditionally used fluorescent labels satisfy all of the necessary requirements for photostability, biocompatibility, brightness, ease of targeting, and multiplexing capability. To this end, the use of combinatorial labeling[2, 3] of biological targets or spectral unmixing algorithms[7, 8] based on fluorescent brightness and even differences in photostability have been demonstrated to great effect to achieve multiplexed imaging.

Fluorescent nanodiamonds (FNDs) containing color centers are biocompatible fluorophores which exhibit infinite photostability, robust chemical stability, and readily functionalizable surfaces for targeted delivery in biological applications.[9, 10-12] Fluorescence in diamond originates from atomic defects within the crystalline lattice. Hundreds of such optically active centers have been and continue to be identified.[13, 14] However, their use in true multiplexing applications has been limited to demonstrations of dual-modal imaging with either red and green emitting FNDs using cathodoluminescence[15] or red and infrared emitting FNDs.[16] This lack of previous extension into multiplexing applications is primarily due to the difficulty in producing more

structurally complex defect centers which emit in the visible and near-IR spectral regions. The majority of focus has been on the nitrogen vacancy (NV), nitrogen-vacancy-nitrogen (NVN, or H3), and silicon-vacancy (SiV) centers, providing emission in the red, green, and near-IR, respectively. We recently reported a novel rapid thermal annealing (RTA) method of producing multicolor fluorescent diamond particles exhibiting fluorescence across the visible spectrum from blue to red using electron irradiated type Ib high-pressure high temperature (HPHT) synthetic diamond.[17] This method involves heating and cooling irradiated diamond particles to predetermined high temperatures very rapidly (on the order of seconds to a few minutes) such that the simultaneous diffusion of specific atomic species (e.g. vacancies and nitrogen) can be facilitated and more precisely controlled as compared to traditional annealing approaches, resulting in a more defined formation of specific color centers or combinations of multiple types of color centers within particles. As a result, the formation of more structurally complex color centers, such as the three-nitrogen vacancy (N3 center) complex, providing blue fluorescence, or the two-nitrogen vacancy (NVN center) are possible. Importantly, these results were achieved in type Ib synthetic diamond. Previously, the formation of N3 and NVN centers was only possible in type Ia natural diamonds, which imparts inherent unpredictability as a result of their origin.

While our earlier efforts were primarily in the demonstration of the RTA technique on particles greater than 10 µm in size,[17] the present manuscript demonstrates an extension of this technique to the nanoscale, with particular emphasis placed on the materials characterization as well as demonstrations in a multiplex imaging experiment. Herein we report the synthesis, characterization, and demonstration of multicolored FNDs exhibiting green, yellow, and red fluorescence in particles less than approximately 150 nm in size. The capability of producing nanoscale blue fluorescent diamond particles is demonstrated in brief. Evaluation of the particles' photoluminescence characteristics at both the ensemble and single particle level is performed, as well as demonstration with a simple labeling experiment with poly(styrene) microbeads and *in vitro* cellular imaging.

2. Experimental

2.1. Synthesis

Synthetic type Ib high-pressure high-temperature (HPHT) diamond particles with initial substitutional nitrogen content of ~100 ppm were used for the production of all fluorescent colors in this study. Particles were irradiated with high energy electrons (3 MeV) to fluences of $1x10^{19}$ e/cm^2 to generate vacancies, and subsequent various annealing approaches were used to generate specific color center combinations. Red, green, and yellow fluorescent diamond particles were all prepared from 100-140 nm starting particle sizes. Blue fluorescent diamond particles were prepared from milling of 15-25 µm particles. Red fluorescent diamond particles were prepared by annealing at 850 °C for 2-hours under vacuum to form NV centers, as is well established in literature.[18, 19] Green, yellow, and blue fluorescent particles were annealed using our previously reported[17] RTA approach at 1800 °C for 2 min., 1700 °C for 3 min., and 1900 °C for 4 min., respectively. Subsequent oxidation using standard procedures well-established in literature[20, 21] was used to remove graphitic carbon and provide a carboxylated (-COOH) terminal surface chemistry on the particles.

For reference in substrate based analysis, natural diamond (Natural green fluorescent diamond particles) of approximately 140 nm prepared via helium ion beam irradiation were used.[22] These particles were only used as a comparison between the green fluorescent particles generated from the RTA technique versus natural diamond (as is typically used in the production of green fluorescent diamond particles). In particular, the fluorescence uniformity and contributions of NV versus H3 fluorescence was investigated with substrate based analyses.

2.2. Photoluminescence Characterization

Photoluminescence characterization consisted of in-solution based as well as substrate based (dry particles on substrate) analyses. Details of the experimental setups for each approach are described separately below.

2.2.1. Solution Based Photoluminescence Characterization

Characterization of fluorescence of the various particles suspended in deionized water consisted of: (1) fluorescent brightness comparisons against standard organic dyes at both equal molar and equal mass concentrations, (2) excitation dependent fluorescent emission spectra, , and (3) fluorescence lifetime characterization.

Commented [N1]: Moved order for consistency with presentation in R&D section.

Fluorescence emission spectra were collected with either laser excitation (WhiteLase SC400, NKT Photonics, UK) at 400 nm (23.6 mW), 450 nm (34.2 mW), 500 nm (47.5 mW), and 550 nm (49.7 mW) or with broad excitation from a mercury lamp using 350/50 nm (UV excitation) (UV-2A filter cube, Nikon), 470/28 nm (blue excitation) (Semrock), or 517/20 nm (green excitation) (Semrock) excitation filters with long pass 420 (Nikon), 488 (Semrock), and 561 (Semrock) nm filters, respectively. In the case of laser-based excitation, spectra were collected with an Ocean Optics Flame spectrometer (Ocean Optics, Germany). Spectra from the mercury lamp excitation source were collected with an Ocean Optics HR2000 USB spectrometer affixed to a widefield Olympus IX-71 inverted epifluorescence microscope. In the case of **Figure 2d**, spectra of solutions under broadband UV excitation (350/50) were collected with an Acton SP2150 Spectrometer (Princeton Instruments). Specific integration times used are noted in the discussion section or in the supplementary information where appropriate.

Brightness comparisons were performed for red and green FND against standard organic dyes. Alexa Fluor™ 647 (AF647) and Fluorescein (Sigma-Aldrich) were used for comparison to the red and green fluorescent diamonds, respectively, by integrating over the corresponding fluorescence spectra. Comparisons were done at both equal weight and equal molar concentrations. Nominal particle sizes of 120 nm and 140 nm were assumed (based on dynamic light scattering, DLS) for the red and green FNDs, respectively, both at concentrations of 0.1 mg/mL in deionized water. AF647 was prepared in deionized water, and fluorescein was prepared in 10 mM sodium hydroxide (NaOH) due to its poor solubility at neutral pH. The green FNDs and fluorescein were excited at 450 nm, with emission collected from a 500 nm long pass filter (all filters from Edmund Optics), whereas the red FNDs and AF647 were excited at 550 nm and 600 nm,

respectively, with the FND emission collected through a 600 nm long pass and dye emission without a filter. Additional details related to the brightness comparison are shown in table S1 (Supplementary Information).

Lifetime measurements were collected for the red and green FNDs and compared against the aforementioned organic dyes. All samples were prepared, excited, and their fluorescence collected as described above. The yellow FNDs were also suspended in DI water (0.1 mg/mL) and analyzed for 450 nm and 550 nm excitation, as they contain a mixture of red and green emitting color centers. Fluorescence decay traces were collected using a single photon counting avalanche photodiode (SPCM-AQRH-XX-TR, Excelitas, USA) and a correlator card (PicoHarp260, PicoQuant, Germany) synchronized to the laser excitation pulses at 5 MHz repetition rate. Lifetime values were determined from double exponential (FNDs) and single exponential (dyes) fits to the decay traces as previously reported.[23] Due to a low amount of available material, the 'fancy blue' particles were not characterized for lifetime.

2.2.2. Substrate-Based Particulate Photoluminescence Characterization

For substrate-based characterizations, an additional control sample of green FNDs produced from type Ia natural diamond (NAT-green) - to serve as a reference to the RTA synthesized green FNDs – was included. Our previous work characterized solution-based photoluminescence spectra of RTA synthesized green FNDs from type Ib diamond as compared to green FNDs from type Ia diamond.[17] Suspensions of red, yellow, green, and NAT-green FNDs (~0.25 mg/mL) were sonicated for 1 min, and poly(vinyl alcohol) (Mowiol® 4-88, *Aldrich*) was added to each suspension to yield a final concentration of 0.15% (w/v). For each sample, 20 µL volumes were spin coated (3000 RPM/30 sec, SC-950P, *essol*) on plasma cleaned gridded coverslips (Grid-50, *ibidi*) and air dried. All samples were imaged with a Yokogawa spinning disk CSU-W1 Confocal Scanner Unit and an Andor Borealis laser illumination system mounted on a Leica TCS SP8 microscope base. A 63x/1.2 NA water immersion objective and a Zyla 4.2 sCMOS camera (*Andor Technology*) were used for imaging. All lasers were used at 100% power, and

frame acquisition time was 200 ms. Presented brightness is corrected based on laser intensities measured above an objective lens, and the following emission filters used (*Semrock*): 450/50, 525/25, 600/50 and 810/90 nm. This correction was not intended to produce qualitative results, but to roughly account for differences in detection efficiency between channels.

For correlative analysis, topographic images of FNDs in the same fields that were imaged as described above were collected with an atomic force microscope (AFM) (Cypher VRS, *Asylum Research*) operating in tapping mode in air using an OTESPA-R3 probe (*Olympus*) after each coverslip was trimmed with a diamond scribe tip and glued to the appropriate sample holder. Image alignment and analysis was performed using ImageJ, ThunderSTORM[24] (default settings with peak intensity threshold set to 5), and Matlab. See the Supplementary Information for source code and additional information.

Additionally, low temperature substrate-based analysis at 70 K was performed on silicon substrates…

Commented [N2]: Philipp, can you add the appropriate information here? I think we can decide on which figures to include as well. Definitely the green diamond at 70 K is interesting, probably only the 475 nm excitation is necessary, and we can put the rest in the SI.

Characterization of the blue FNDs consisted of only particulate based photoluminescent spectroscopy using the aforementioned Olympus IX-71 epifluorescence microscope with UV excitation (350/50 nm) and long pass emission filter (405 nm).

2.3. Imaging Demonstrations

2.3.1 Polymer Bead Labeling

The goal of this experiment was to demonstrate labeling of the surface of a feature size to approximate that of a cell. Carboxylated red, yellow, and green fluorescent diamond particles synthesized via the rapid thermal annealing treatment were attached to SuperAvidin™ coated microspheres (SA-beads) (*Bangs Laboratories Inc., USA*) having nominal diameters of 15.3 µm. For each of the individual three colors, the labeling procedure was as follows: 25 µL of the SA-Bead solution, supplied at 10 mg/mL in 0.1M PBS with antibacterial additives, was diluted to 250 µL with 0.1M PBS and subsequently washed 3x with centrifugation (6,000 RPM/5 min., Spectrafuge). After the third wash, the

SA-beads were resuspended in 0.1M PBS to a concentration of 1 mg/mL. To 1 mL of this SA-bead solution, 1 mL of poly(ethylene glycol) 2-aminoethyl ether biotin (Biotin-PEG-Amine, Average M_n = 2,300) (*Millipore Sigma, USA*) at 1 mg/mL in 0.1M PBS was added. The solution was then incubated for 30-minutes at room temperature on a shaker plate. After incubation, the SA-beads were centrifuged at 6,000 RPM/3 min. and reconstituted into 1.8 mL of deionized water.

Separately, 2 mL suspensions at ~0.25 mg/mL in deionized water of each of three colors of diamond particles were pelleted with centrifugation at 14k RPM/10 min. The particles were reconstituted into 1 mL of dry dimethylformamide (DMF, *Millipore Sigma, USA*) and pelleted once more at the same centrifugation conditions before a final reconstitution into 1 mL of dry DMF. This second pelleting was done to ensure removal of residual water. A 100 mg/ml stock solution of 1,1'-Carbonyldiimidazole (CDI, *Millipore Sigma, USA*) was prepared in dry DMF, and 1 mL of this suspension was added to three 2-mL microcentrifuge tubes. These solutions were then incubated for one hour each on a shaker plate. After the one-hour CDI-activation of the diamond particles was completed, they were pelleted at 14k RPM/10 min., and reconstituted in to approximately 100 µL of dry DMF, before being added to each of the three prepared solutions of SA-beads (one for each of the respective colors of diamond particles used). The combined SA-beads and diamond solutions were incubated overnight at room temperature on a shaker plate. The following day, the FND-labeled SA-beads were washed with 1% bovine serum albumin (BSA) in PBS until unconjugated diamond was removed to as high of a degree as possible for suitable fluorescence imaging. This labeling approach can lead to labeling of the amines on the biotin as well as the streptavidin directly, leading to a higher labeling density overall. As a control experiment to determine, qualitatively, the uniformity of SA coating on the microbeads, a separate solution of SA-beads (the same amount as used with diamond labeling) was incubated with excess Cyanine-5-Biotin (cy5-Biotin) for 30 minutes and subsequently washed and imaged.

Microscopy of the labeled beads was performed with an Olympus IX-71 inverted epifluorescence microscope with a mercury lamp excitation. 10 µL droplets of the labeled beads were placed on coverslip glass (Gold Seal™, *Thermo Fisher, USA*) for imaging.

Micrographs were captured with a 5-Megapixel CCD fluorescence microscope camera (MT5000-CCD, AmScope, USA). Different emission filters were used depending on the specific instance of imaging, and are thus specifically noted in figures and in the discussion section where appropriate. All filters and dichroics used for these experiments are listed in table S2 (Supplementary Information). Images were taken at different magnifications (10x, 40x, 100x, or 160x), and these are noted specifically in figure captions and in the discussion section. Specific details of the models and types of objective lenses used are listed in table S3 (Supplementary Information).

2.3.2 Multiplex cell imaging of green and red FNDs

Two sets of MDA-MB-231 cells (Human breast adenocarcinoma) were cultured separately in Dulbecco's modified Eagle's medium (DMEM) supplemented with 10% fetal bovine serum, 2mM L-glutamine, and 1% penicillin-streptomycin (v/v). 40 µg/ml of each FNDs (green and red) particles were added separately to each set of cells and incubated for 24h. Then, the cells were washed 3 times with PBS and trypsinized. The trypsinized cells of each group (cells incubated with green or red FNDs) were then mixed and added to glass coverslips. These cells were then incubated overnight to adhere, and the cells were then fixed in 4% PFA (paraformaldehyde) for 10 minutes. The cells were washed 3 times with PBS and mounted over glass slides with mounting medium containing VECTASHIELD and DAPI (4′,6-diamidino-2-phenylindole). The confocal microscopy set up consisted of LSM 780 (Zeiss, Germany), 63X water objective and PMTs (Photomultiplier tubes). The cell sample was first excited by a 488nm argon laser and emission was collected at 510-550 nm and 650-740 nm for green and red FNDs respectively. Subsequently, the same field of view was excited by a 543 nm laser and emission settings of green and red channels were kept the same. DAPI was excited with 405nm laser and emission was collected in 410-450 nm.

2.3.3 Confocal cell imaging of Yellow FNDs

MDA-MB-231 cells (Human breast adenocarcinoma) were cultured in Dulbecco's modified Eagle's medium (DMEM) supplemented with 10% fetal bovine serum, 2mM L-glutamine, and 1% penicillin-streptomycin (v/v) over glass coverslips. 10 µg/ml of Yellow FNDs particles was added to cells. The cells were incubated with Yellow FNDs for 24h. Cell samples were fixed with 4%PFA and mounted over glass slides with ibidi mounting medium (Ibidi, Germany). The confocal microscopy set up consisted of TCS SP5 (Leica Microsystems, Germany), 100X oil objective, LAS AF imaging software and PMTs (Photomultiplier tubes). The cell sample was imaged by sequential scanning. The sample was first excited by a 488nm argon laser and emission was collected at 510-550 nm. Later a 561 nm diode laser was used for excitation and emissions were collected at 567-590 nm (yellow) and 650-740 nm (red). Phase contrast images were used to visualize the cells.

3. Results & Discussion

3.1 Synthesis

Our previous work discussed many of the aspects related to the RTA treatment on electron irradiated particulate diamond;[17] therefore, an extended discussion on the specifics of the synthesis technique is avoided. Generally, the observations of our previous work are confirmed in this study as well with smaller particle sizes. In particular, at annealing temperatures above approximately 1700 °C, significant changes in the luminescence become apparent due to the onset of radiation-stimulated diffusion of Nitrogen. Importantly, this annealing technique is again demonstrated as suitable for even reasonably small particulate sizes on the order of 100 – 140 nm in diameter for the formation of NV, H3 (NVN), and N3 color centers providing red/orange, green, and blue fluorescence, respectively, in type Ib synthetic diamond (See figure S1, Supplementary Information, for particle size distributions of red, green, and yellow FNDs used in this study).

During rapid annealing, combinations of these various color centers can potentially form and result in diamond particulates exhibiting fluorescence across the visible spectrum. In the case of this work, the yellow FNDs are representative of a combination of NV and H3 centers, providing a combination of red/orange and green fluorescence, thereby resulting in a net yellow fluorescence under appropriate excitation conditions.

3.2 In-Solution Based Photoluminescence Characterization

A comparison of fluorescent brightness intensity based on integration of emission spectra are shown in **Figure 1**. The brightness comparisons at equal weight (mass) concentrations as well as equal molar concentrations are consistent with previously reported comparisons between fluorescent diamond and organic dyes.[25] [26] Namely, in the equal weight consideration, Fluorescein (FITC) and Alexa 647 are approximately four orders of magnitude brighter than green and red fluorescent diamonds, respectively. This is a result of the fact that a single diamond particle is of significantly higher mass than a single dye molecule; therefore, we are effectively comparing many millions of dye molecules with a single diamond particle. In the equivalent molar consideration, which is equivalent to comparing one dye with one FND particle, the green and red fluorescent diamonds are effectively two and three orders of magnitude brighter than FITC and Alexa 647, respectively. In this case, it is important to consider that each diamond particle contains a relatively high density of fluorescent centers (H3 or NV centers for green or red diamonds, respectively) per unit volume. The combination of multiple color centers within single diamond particles was previously demonstrated to provide higher intensity fluorescence as compared to organic dyes. [26] Moreover, in the equal molar consideration, the molarity comparison is based on the molarity of diamond particles as compared to the molarity of dye molecules. This is an important consideration, because, in the case of diamond, it is not the particle itself that fluoresces, but the color centers encapsulated within the diamond lattice. Thus, the higher effective molar brightness of the diamond particles can be explained by the considering that a single diamond particle containing several hundreds of color centers will exhibit higher brightness than a single dye

molecule. We note that the yellow FNDs were not considered for this comparison, because, unlike a typical yellow dye (e.g. Rhodamine 6G), the yellow FNDs are a combination of red and green fluorescence emission from NV and H3 centers. Thus, a direct comparison to a yellow fluorescent dye is less instructive table S1 (Supplementary Information) contains the quantitative parameters used for brightness comparison.

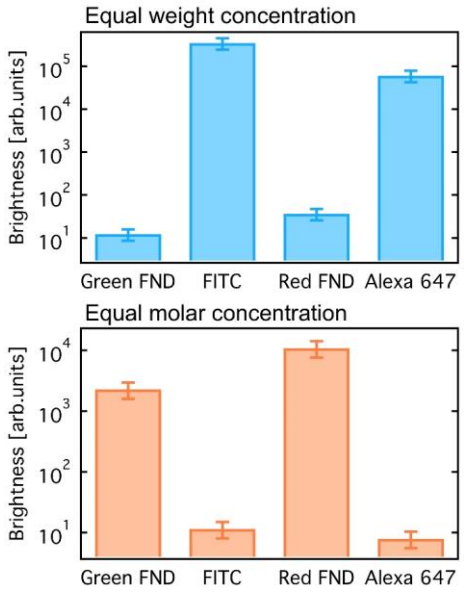

Figure 1. *Fluorescence brightness comparison between green and red fluorescent diamonds (140 nm) against the common organic dyes fluorescein (FITC) and Alexa 647 estimated for equal mass (top) and equal molar (bottom) concentrations.*

Figure 2a-c demonstrates the laser excitation wavelength (λ_{ex}) dependence of the fluorescence of each diamond type, and **Figure 2d-e** show the emission spectra for each diamond type collected under UV excitation (360 nm) using an optical long pass (405 nm) filter and blue excitation (470/28 bandpass) using an optical long pass (488 nm) filter. In the case of laser excitation, Raman scattering from water becomes pronounced as lower excitation wavelengths (particularly at 400 nm). Figure S2 (Supplementary Information) shows water Raman scattering spectra for all laser excitation wavelengths. Excitation of

the diamond particles in solution with 400 nm is particularly skewed by the water Raman, and is shown in Figure S3 (Supplementary Information). Figure S4 (Supplementary Information) directly compares the effect of different excitation wavelengths on the FND fluorescence spectra based on the data plotted in **Figure 2a-c**. A close examination of the emission spectra reveals several interesting characteristics of each of the diamond particle types, and each is now discussed separately.

The green FNDs, as expected, exhibit a predominance of H3 related emission centered around 520 nm emission under 450 nm excitation. An optical filter cuts off this emission below 550 nm in the case of 500 nm excitation; however, there is a clear shoulder extending upwards attributed to the H3 center. Under 550 nm excitation, the green FNDs still exhibit detectable amounts of NV related fluorescence. This is expected given the high thermal stability of NV centers observed with previous RTA treatments of diamond.[17] From a materials engineering perspective, it may be challenging to completely remove all NV centers because of their temperature stability and graphitization that can occur when holding the particles at high temperature at atmospheric pressure for extended times. However, it is possible reduce their concentration in the diamond lattice to levels below the detection limit under specific imaging conditions. For example, in the case of broadband blue excitation (**Figure 2e**), the NV related emission is effectively undetectable. Demonstrations with confocal optical microscopy illustrate this point further (see Section 3.4).

The yellow FNDs exhibit a combination of emission from H3 and NV centers, most apparent under 450 nm excitation. However, the relative brightness of the yellow particles is significantly lower than that of the green particles under 450 nm excitation (**Figure 2a**). Notably, under 400 nm excitation, the majority of the signal collected below 550 nm in the yellow FNDs may be attributed to water Raman scattering. However, there is a more pronounced shoulder in the yellow FNDs from approximately 500-550 nm in comparison to the red FNDs, and this is attributed to H3 centers (Figure S3, Supplementary Information). Moreover, the green FNDs exhibit a well pronounced peak under the same excitation. This suggests that the relative amounts of H3 centers in the yellow FNDs are lower in comparison to the green particles, since an increase in the H3 contribution will

lead to dominant green fluorescence. Yellow light can be made by an approximate 50/50 mix of red and green light; thus, it might be expected that under the appropriate excitation and emission conditions, the spectral intensities of fluorescence contribution from NV and H3 centers would be approximately similar in the case of the yellow particles. This would appear to be the case in **Figure 2e** under broadband blue excitation. Nevertheless, it is important to note that observed fluorescence emission is strongly excitation wavelength dependent (**Figure 2a-c**), and the observed fluorescence of the yellow FNDs in particular can change dramatically depending on the excitation wavelength and optical filter set used. In comparing 500 and 550 nm excitation (**Figure 2b,c**), the yellow diamond exhibits a lower amount of NV(0) related fluorescence (shoulder from approximately 550 nm to 625 nm) than the red diamond particles. Thus, the relative NV(0) contribution is apparently higher in the red FNDs as compared to the yellow FNDs. This may be explained by either a structural difference or processing difference in the yellow FNDs. Structurally, the presence of H3 centers may affect NV(0) emission. From a processing standpoint, the red FNDs were annealed at a much lower temperature (850 °C) compared to the 1700 °C temperature of the yellow FNDs, and the higher temperature annealing clearly affects defect center configurations.

A similar effect can be seen under 360 nm UV excitation (**Figure 2d**). While the shoulder associated with the H3 center is observed in both the red and yellow FNDs, it is more pronounced in the yellow FNDs than the red FNDs, and both are significantly lower in comparison to the H3 peak observed for the green FNDs. Under blue excitation (**Figure 2e**), the H3 related peak is more pronounced in the yellow FNDs as compared to the same diamonds under UV excitation (**Figure 2d**). This is due to the weak excitation efficiency of H3 centers with 360 nm excitation source as compared excitation lines closer to 480 nm (e.g. the blue excitation used in **Figure 2e**). Interestingly, NV(0) absorption extends all the way to the bandgap energy (5.6 eV, ~220 nm),[13] which explains why the NV(0) contribution is still so pronounced under UV excitation.

Lastly, the appearance of a weak shoulder from approximately 530-580 nm in the red FNDs under blue excitation (**Figure 2c**) is a shorter wavelength component of the NV(0) center.

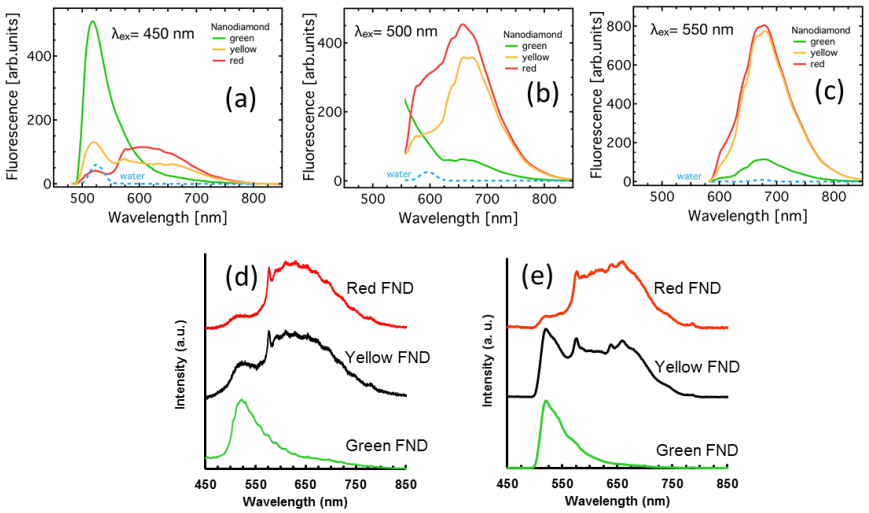

Figure 2. *(a-c) Excitation wavelength dependent fluorescence spectra of green, yellow, and red FNDs suspended in water (0.1 mg mL^{-1}) for laser excitation at 450 nm, 500 nm, and 550 nm. (d-e) Fluorescence spectra for red, yellow, and green FNDs under broadband UV excitation (panel d, 360 nm, 0.8 s. integration time) and blue excitation (panel e, 470/28 nm , 3 s integration time)using a widefield fluorescence microscope. Blue excitation (panel c) was achieved using a FF01-470/28 band pass excitation filter (Semrock) and fluorescence collected through a BLP01-488R long pass emission filter (Semrock). Spectra have been normalized for intensity values to range between 0 and 1 and then adjusted vertically for ease of comparison. It should be noted that the spectrometer used to collect the spectra in panel d provides higher resolution than the one shown in panel e, hence the spectroscopic features appear sharper in comparison.*

Figure 3 shows the fluorescence lifetime of the red and green diamonds in comparison to standard dyes. The dyes exhibit lifetimes on the order of literature reported values [27]. The green diamonds (H3 center) exhibit longer fluorescence lifetimes than the red diamonds (NV center), which has previously been shown in literature.[28-31] The lifetime value of 21.8 ns determined here for the green FNDs (H3 center) differs from previously reported lower value of 16 ns for the H3 center in bulk diamond.[28] However, precedence for increased lifetimes from the NV center has been shown in nanoparticles as compared to bulk diamond.[32] The significant difference in fluorescence lifetime of green and red

FNDs implies that fluorescence lifetime imaging microscopy (FLIM) can be used to enhance contrast between red and green diamonds. In general, fluorescence lifetime imaging has previously been demonstrated with the NV center in particular.[31, 33]

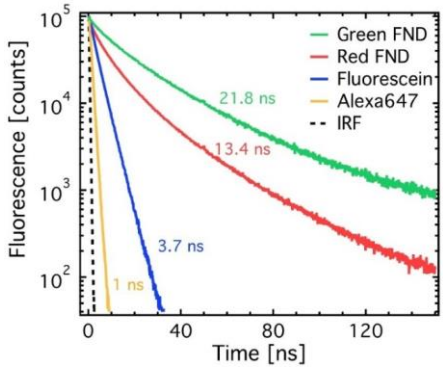

Figure 3. *Fluorescence lifetime plots of green and red diamonds as compared to Fluorescein (FITC) and Alexa 647, respectively.*

3.3 Substrate-Based Particulate Fluorescence Characterization

While in-solution based photoluminescent spectroscopy generates a wealth of information with respect to the average luminescence of many particles, substrate based particle characterization is an important consideration. Inhomogeneous FNDs used as targeted fluorescent labels for cells or other biological features can complicate identification and imaging, particularly at higher magnifications. Due to processing, even state-of-the-art fluorescent nanodiamonds exhibit some degree of non-uniformity. This non-uniformity can arise from the starting material, processing conditions, and particle size and shape, among other factors.[23] Novel irradiation approaches have been demonstrated as a means to improve fluorescence uniformity,[34] and the RTA approach may offer a unique post processing step to facilitate higher particle fluorescence uniformity, or, at the very least, brighter particles, which are also greatly needed.

From **Figure 4**, several observations can be made: (1) The red FNDs exhibit the brightest fluorescence in the far-red channels, (2) the yellow FNDs also exhibit high

brightness in the far-red emission channel; however, they also exhibit higher fluorescence in the green channel under 488 nm excitation as compared to red FNDs. Thus, the yellow FNDs apparently contain both NV and H3 centers, which is consistent with the in-solution base spectroscopy. (3) Comparison between the RTA synthesized green FNDs versus the green FNDs synthesized from natural diamond indicates that the RTA treated green FNDs containing H3 centers show more intense green fluorescence compared to natural diamonds containing H3 centers. They also exhibit more NV related fluorescence in comparison to the natural diamonds. The higher brightness observed in the RTA synthesized green FNDs can be associated with the lower nitrogen content of type Ib diamond compared to type Ia natural diamond. It has previously been observed that increasing nitrogen content can suppress both the luminescence intensity as well as the fluorescence lifetime of the H3 center in diamond.[35, 36] In particular, the effects of high nitrogen content in the form of A centers (N-N pairs) on lattice strain fields has been suggested as a mechanism for this quenched emission.[35] The presence of NV centers in the RTA treated sample is also an indication of the very high temperature stability of the NV center, which can persist even a very high temperatures once formed.[13] Figure S5 (Supplementary Information) contains a complete picture of all excitation/emission combinations used for this substrate based analyses as well as intensity normalized AFM-confocal images. Figure S6 (Supplementary Information) shows the emission intensity of fluorescent particles as a function of size as determined by correlative AFM and spinning disk confocal microscopy.

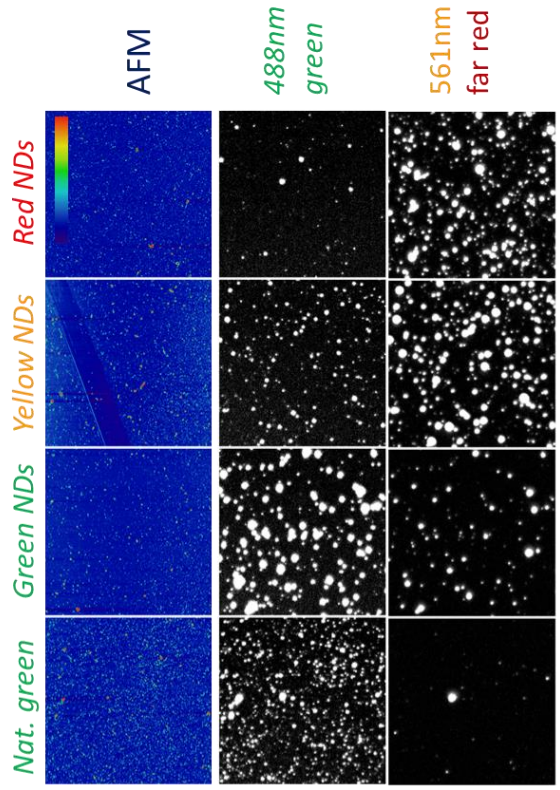

Figure 4*: Correlative fluorescence microscopy and AFM of individual FNDs (red, yellow, green, NAT-green). Each field of FNDs was imaged with a spinning disk confocal microscope at different combinations of excitation laser and emission collection channels. For each excitation/emission combination, gray-levels are scaled up to present estimates of relative brightness per unit laser power per unit of emission bandwidth. See experimental section for details of grayscale adjustment. Emission bands are typical spectral ranges used on commercial microscopes to collect "green" (e.g., GFP) and "far red" (e.g., AF647). Each square is 30 µm x 30 µm. The color range in the AFM field (violet to red) corresponds to a height of (0-100 nm). Light microscopy contrast is adjusted to present the brightest particles.*

Lastly, **Figure 5** demonstrates the possibility of 'fancy blue' fluorescent diamond particles. Fancy blue particles contain a mixture of N3 and H3 centers, and give an

aquamarine fluorescence under UV excitation which is distinct from that of particles containing predominantly H3 centers. Importantly, this fancy blue fluorescence does not appear to be significantly altered upon fragmentation, and this suggests the possibility of achieving nanoscale sized FNDs with a new and distinct fluorescence that was not previously achieved at that size scale. For this study, only a very small amount of the fancy blue material was produced, thus, a more extensive evaluation of the material was not performed, but will be the subject of future studies.

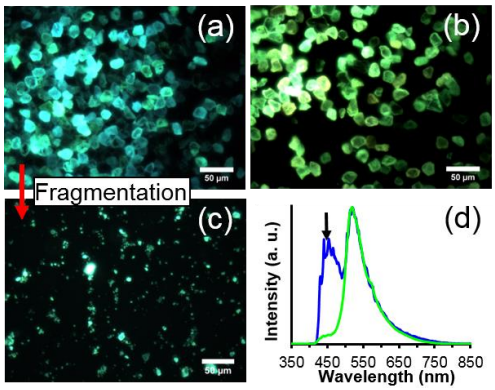

Figure 5. *(a) 'Fancy blue' particles before fragmentation under UV excitation at 40x magnification. (b) Green particles under similar UV excitation, illustrating difference in visible emission. (c) 'Fancy blue' particles after fragmentation under UV excitation. (d) Photoluminescent spectra of 'fancy blue' versus green particles under UV excitation, with blue particles demonstrating an enhanced shoulder below 500 nm consistent with N3 centers.*

3.4 Imaging Demonstrations

Figure 6 illustrates that three distinct colors – green, yellow, and orange – can be observed from each of the three diamond types (green, yellow, and red, respectively) under a single broadband blue excitation. The orange appearance of the red diamonds is due to preferential emission of NV(0) centers at this excitation wavelength. It should be noted that blue excitation is preferentially suited for the green diamonds, and this in reality causes the emission intensities of the red and yellow diamonds to be lower; however, it is still possible to distinguish the three colors by eye.

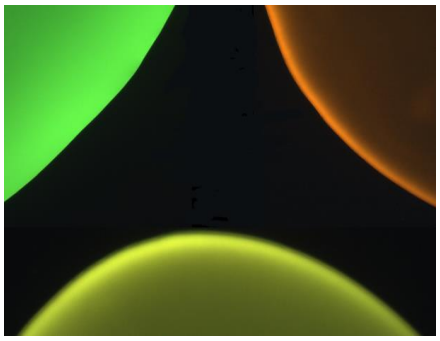

***Figure 6**. Droplets of green (top left), red (top right), and yellow (bottom) fluorescent diamonds of approximately 140 nm in size in deionized water at approximately 1 mg/mL. Fluorescence observed under short arc mercury excitation with a FF01-470/28 band pass filter (Semrock) and emission through a BLP01-488R long pass filter (Semrock) for all diamond types. Note that the exposure times differ with each droplet in the image (this is a single image stitched from three images) to provide roughly equalize brightness. The color images were collected using a color camera and therefore reflect the actual fluorescence color with no pseudo coloring.*

SA-Microbead Labeling:

The primary goal of the polymer bead labeling experiment was to demonstrate the capability of using the green, yellow, and red diamonds for multicolor imaging on feature sizes comparable to cells. As noted in the experimental section, the particular route of labeling used in these experiments could have led to non-specific labeling of amines on the streptavidin in addition to the amine coupled to the Biotin-PEG-Amine molecule. However, it is again stressed that the goal was imaging contrast and not labeling specificity or validation. Validation of bead activity and streptavidin uniformity was performed using a cy5-Biotin control (see figure S7, Supplementary Information).

Figure 7 depicts the FND labeled SA-Beads under broadband blue excitation (**Figure 7c**) and broadband green excitation (**Figure 7d**) using the filters shown in **Figure 7a** and **Figure 7b**, respectively. Under blue excitation, clear delineation between green labeled and red or yellow labeled beads is observed. Discerning red FND and yellow FND labeled beads under blue excitation is more challenging, with the red labeled beads

exhibiting a slight orange as opposed to a stronger yellow fluorescence. Under green excitation, the contribution from green FND labeled beads is strongly diminished; however, it is slightly brighter than the autofluorescence of the starting beads, indicating a small amount of NV related contribution from the green FNDs, which is validated spectrally. Red FND and yellow FND labeled beads are of similar brightness under green excitation. The slight 'halo' effect observed surrounding the beads is indicative of surface labeling of the beads. This does mean that the predominantly green autofluorescence from the bulk of the beads can contribute to the observed coloration to some extent.

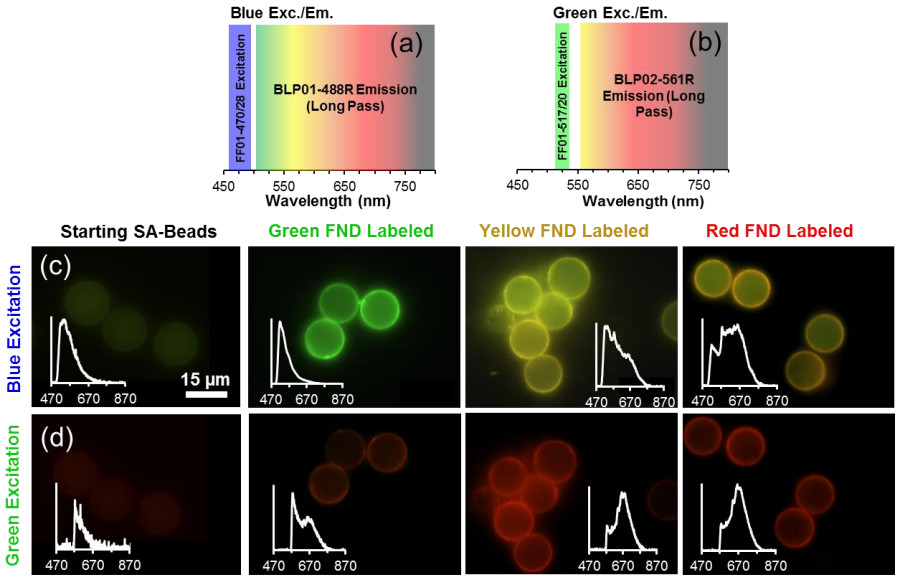

Figure 7. *Excitation and emission filter sets used for image capture of labeled beads under blue excitation (a) and green excitation (b). (c) Micrographs of starting SA-beads and green, yellow, and red FND labeled beads under blue excitation shown in (a). (d) Micrographs of starting SA-beads and green, yellow, and red FND labeled beads under green excitation shown in (b). All images taken at 100x magnification.*

A consequence of the intrinsic bead autofluorescence and the relatively weak H3 related fluorescence in the yellow particles is that they inhibit the ability to clearly separate yellow

from red labeled beads under blue excitation when the separately labeled beads are mixed and observed in the same field of view. An attempt was made to use band pass filters for differentiation; however, this was not successful due to the autofluorescence of the beads. Nevertheless, it was clear which beads were labeled with green FND particles, given their significantly higher emission intensity under blue excitation. The band pass filter spectral results are summarized in figure S8 (Supplementary Information).

Spectral validation to confirm the presence of diamond on the beads was performed and is inset within the micrographs (**Figure 7c-d**).The spectral profiles clearly demonstrate the presence of diamond, with typical profiles and spectral characteristics for NV centers such as the zero phonon lines (ZPLs) at 575 nm and 638 nm. Although intensity values are not shown on the inset plots, the green FND labeled beads exhibited an order of magnitude higher fluorescent intensity as compared to the starting beads exhibiting autofluorescence.

Cell Imaging:

Cellular imaging of MDA-MD-231 cells that were incubated with red and green diamond particles are shown in **Figure 8**. In this case, cellular uptake is non-specific, with no specific targeting ligand. **Figure 8a** summarizes the experimental approach used for demonstrating dual color imaging. Two cell cultures of MDA-MD-231 breast cancer cells were incubated separately with either red or green FNDs, and then the cultures were mixed together for fluorescence imaging. **Figure 8b** shows the excitation lines and emission bands used for imaging. **Figures 8c-f** show cellular fluorescence imaging under specified excitation and emission conditions listed on each image. Note that a DAPI stain for cell nuclei was imaged under 405 nm excitation, and is shown in all image panels. From **Figure 8**, two important observations can be made: (1) under 488 nm excitation, red and green fluorescent diamond particles can be differentiated easily, (2) there is insignificant fluorescence 'bleed through' in these imaging conditions. Observation (1) is a result of the large Stokes shift difference between red and green fluorescent diamond particles, and is evident in **Figure 8c-e**. Observation (2) is an important conclusion given

the small amount of spectral overlap between red and green diamond particles given the apparent presence of small amounts NV centers in the green diamond (**Figure 2c, Figure 4**). This is also evident in **Figure 8f**, where minimal NV related fluorescence can be observed to be emitting from the green FND particles.

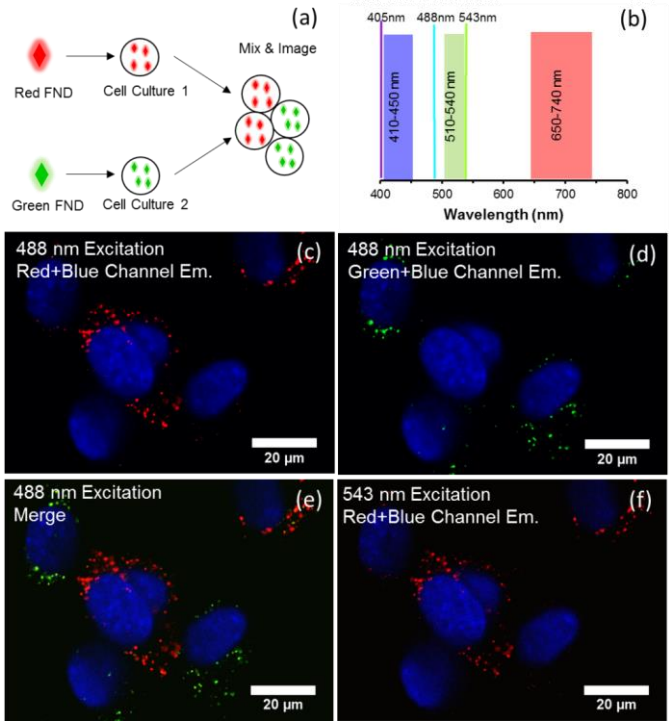

Figure 8: *Confocal imaging of cells labeled separately with green FNDs and red FNDs under 488 nm excitation and 543 nm excitation. (a) Schematic of experimental approach for dual color imaging. (b) Excitation lines and emission windows for collected images. Note that the DAPI stained nuclei were excited under 405 nm, and is the only use of this excitation line in all images. (c-f) 488 nm excitation with emission collected from the red channel (650-740 nm) (c), green channel (510-550 nm) (d), and a merge of both channels (e). (f) Red channel emission (650-740 nm) under 543 nm excitation, demonstrating no (or very low) bleed through fluorescence from the NV centers present in green FND particles.*

In contrast to the cell labeling with either green or red FND (**Figure 8**), labeling with the yellow FNDs which contain both NV and H3 centers has distinct behavior. The same particles demonstrate green emission under 488 nm excitation and red emission under 561 nm excitation (**Figure 9**); thus, dual-color emission as opposed to the singular color emission of either red or green FNDS which contain either a dominance of NV or H3 centers, respectively. This dual-color emission allows for differentiation of the yellow FNDs from the background fluorescence. In the "yellow" channel (567-590nm), the particles demonstrate yellow emission.

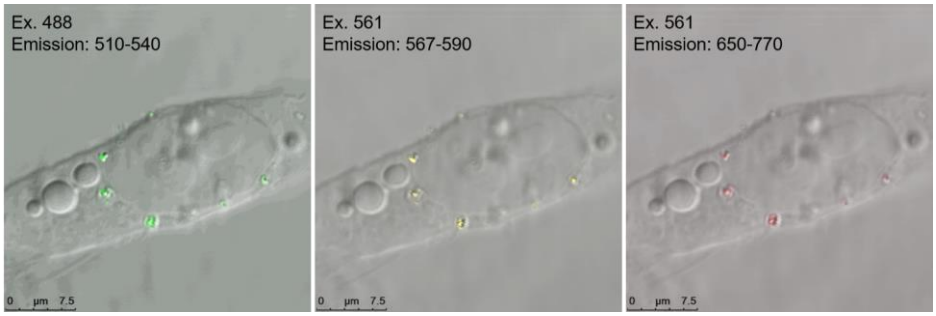

Figure 9. *Yellow diamond particles demonstrating emission in three channels with two different excitation wavelengths.*

Nanodiamond particles with combined red and green emission may find application in correlative light-electron microscopy (CLEM) since they are bright and electron-dense in nature. Therefore, they could be detectable with light in two emission channels and by and electron microscopes. FNDs in general are a well reported probe for STED and STORM microscopy. [6, 37, 38] They could be useful as a fiducial marker for two-color STED-CLEM. In a recent report, super-resolution STED-CLEM has been demonstrated with red FNDs in a combination of green fluorophore.[38] However, yellow FNDs could potentially facilitate CLEM experimental setups with combination of green and red fluorophores since dual color emitting fiducials can be well distinguished, and having a CLEM fiducial marker with an emission distinct from that of a labeling fluorophore is critical for selective identification of labeled features.

4. Conclusions

Herein we reported, to the best of our knowledge, to first use demonstrations of multicolor fluorescent diamond particles in practical imaging modalities (wide field and confocal fluorescence microscopy). Blue and yellow fluorescent diamond particles at smaller size ranges, as well as a practical demonstration of green fluorescent diamond particles synthesized via our previously reported rapid thermal annealing technique were demonstrated. Successful dual modal imaging of a mixture of cells labeled with either green or red fluorescent diamond particles was achieved in confocal cellular imaging. Cells labeled with green FND were visible only in the green channel while cells labeled with red FND could be observed only in the red channel. The yellow fluorescent particles exhibiting spectral combination of both red (NV) and green (H3) fluorescence meant they could be detected simultaneously in green and red channels under corresponding excitation.

While the focus of this work was on the use of these particles in fluorescence labeling and imaging, particles exhibiting combinations of color centers may have significant implications in super-resolution microscopy (see section 3.4) and in magnetic/microwave modulated fluorescence imaging. With regard to modulated fluorescence imaging, it was previously demonstrated that the NV(-) center can be driven to a dark state in appropriate conditions for signal enhancement against an auto fluorescent background.[39] Yellow FNDs containing appreciable amounts of both NV and H3 centers (see section 3.2), may exhibit the possibility of a ‘chromic-shifting’ fluorescent label, whereby the observed emission of the particles can be modulated by suppression or enhancement of the NV(-) center. Beyond biological applications, such a fluorescent material may find application in tracing, authentication, and anticounterfeiting.

Conflict of Interest

The authors declare no conflict of interest.

Acknowledgements

This work has been funded in whole or in part by the National Cancer Institute (NCI) of the National Institutes of Health (NIH) under Award Number R43CA232901, the National Heart, Lung, and Blood Institute (NHLBI), Department of Health and Human Services, under Contract No. HHSN268201500010C, and with Federal funds from the National Cancer Institute, National Institutes of Health, under Contract No. HHSN2612008001E. NP and JR acknowledge funding from the Academy of Finland (Grant No. 309374) and the Sigrid Jusélius Foundation. EK acknowledges support from the NIH Post-Baccalaureate Intramural Research Training Award Program at the National Cancer Institute. The content of this publication does not necessarily reflect the views or policies of the Department of Health and Human Services, nor does mention of trade names, commercial products, or organizations imply endorsement by the U.S. Government.

References

1. B. P. Joshi and T. D. Wang, *Contrast Media & Molecular Imaging*, 2018, **2018**, 1-19.
2. J. Livet, T. A. Weissman, H. Kang, R. W. Draft, J. Lu, R. A. Bennis, J. R. Sanes and J. W. Lichtman, *Nature*, 2007, **450**, 56.
3. E. Lubeck and L. Cai, *Nature Methods*, 2012, **9**, 743.
4. F. Collman, J. Buchanan, K. D. Phend, K. D. Micheva, R. J. Weinberg and S. J. Smith, *Journal of Neuroscience*, 2015, **35**, 5792-5807.
5. X. Wan, R. P. O'Quinn, H. L. Pierce, A. P. Joglekar, W. E. Gall, J. G. DeLuca, C. W. Carroll, S.-T. Liu, T. J. Yen, B. F. McEwen, P. T. Stukenberg, A. Desai and E. D. Salmon, *Cell*, 2009, **137**, 672-684.
6. J. Yi, A. Manna, V. A. Barr, J. Hong, K. C. Neuman and L. E. Samelson, *Molecular biology of the cell*, 2016, **27**, 3591-3600.
7. A. Orth, R. N. Ghosh, E. R. Wilson, T. Doughney, H. Brown, P. Reineck, J. G. Thompson and B. C. Gibson, *Biomedical optics express*, 2018, **9**, 2943-2954.
8. A. M. Valm, R. Oldenbourg and G. G. Borisy, *PLOS ONE*, 2016, **11**, e0158495.
9. H. C. Chang, W. W. Hsiao and M. C. Su, *Fluorescent Nanodiamonds*, Johhn Wiley & Sons Ltd., 2019.
10. W. W.-W. Hsiao, Y. Y. Hui, P.-C. Tsai and H.-C. Chang, *Accounts of chemical research*, 2016, **49**, 400-407.
11. M. Chipaux, K. J. van der Laan, S. R. Hemelaar, M. Hasani, T. Zheng and R. Schirhagl, *Small*, 2018, **14**, 1704263.

12. O. A. Shenderova, A. I. Shames, N. A. Nunn, M. D. Torelli, I. Vlasov and A. Zaitsev, *Journal of Vacuum Science & Technology B*, 2019, **37**, 030802.
13. A. M. Zaitsev, in *Optical Properties of Diamond: A Data Handbook*, Springer Berlin Heidelberg, Berlin, Heidelberg, 2001, DOI: 10.1007/978-3-662-04548-0_5, pp. 125-376.
14. G. Davies, S. C. Lawson, A. T. Collins, A. Mainwood and S. J. Sharp, *Physical Review B*, 1992, **46**, 13157-13170.
15. Y. Nawa, W. Inami, S. Lin, Y. Kawata, S. Terakawa, C.-Y. Fang and H.-C. Chang, *ChemPhysChem*, 2014, **15**, 721-726.
16. K. Bray, L. Cheung, K. R. Hossain, I. Aharonovich, S. M. Valenzuela and O. Shimoni, *Journal of Materials Chemistry B*, 2018, **6**, 3078-3084.
17. L. Dei Cas, S. Zeldin, N. Nunn, M. Torelli, A. I. Shames, A. M. Zaitsev and O. Shenderova, *Advanced Functional Materials*, 2019, **0**, 1808362.
18. G. Dantelle, A. Slablab, L. Rondin, F. Lainé, F. Carrel, P. Bergonzo, S. Perruchas, T. Gacoin, F. Treussart and J. F. Roch, *Journal of Luminescence*, 2010, **130**, 1655-1658.
19. X. Song, G. Wang, X. Liu, F. Feng, J. Wang, L. Lou and W. Zhu, *Applied Physics Letters*, 2013, **102**, 133109.
20. S. Osswald, G. Yushin, V. Mochalin, S. O. Kucheyev and Y. Gogotsi, *Journal of the American Chemical Society*, 2006, **128**, 11635-11642.
21. A.-Y. Jee and M. Lee, *Current Applied Physics*, 2009, **9**, e144-e147.
22. T.-L. Wee, Y.-W. Mau, C.-Y. Fang, H.-L. Hsu, C.-C. Han and H.-C. Chang, *Diamond and Related Materials*, 2009, **18**, 567-573.
23. P. Reineck, L. F. Trindade, J. Havlik, J. Stursa, A. Heffernan, A. Elbourne, A. Orth, M. Capelli, P. Cigler, D. A. Simpson and B. C. Gibson, *Particle & Particle Systems Characterization*, 2019, **0**, 1900009.
24. M. Ovesny, P. Krizek, J. Borkovec, Z. Svindrych and G. M. Hagen, *Bioinformatics (Oxford, England)*, 2014, **30**, 2389-2390.
25. P. Reineck, A. Francis, A. Orth, D. W. M. Lau, R. D. V. Nixon-Luke, I. D. Rastogi, W. A. W. Razali, N. M. Cordina, L. M. Parker, V. K. A. Sreenivasan, L. J. Brown and B. C. Gibson, *Advanced Optical Materials*, 2016, **4**, 1549-1557.
26. N. Mohan, Y.-K. Tzeng, L. Yang, Y.-Y. Chen, Y. Y. Hui, C.-Y. Fang and H.-C. Chang, *Advanced Materials*, 2010, **22**, 843-847.
27. ISS Inc., Lifetime Data of Selected Fluorophores, http://www.iss.com/resources/reference/data_tables/LifetimeDataFluorophores.html, 2019).
28. S. C. Rand and L. G. DeShazer, *Opt. Lett.*, 1985, **10**, 481-483.
29. G. Liaugaudas, A. T. Collins, K. Suhling, G. Davies and R. Heintzmann, *Journal of Physics: Condensed Matter*, 2009, **21**, 364210.
30. G. Liaugaudas, G. Davies, K. Suhling, R. U. A. Khan and D. J. F. Evans, *Journal of Physics: Condensed Matter*, 2012, **24**, 435503.
31. J. Storteboom, P. Dolan, S. Castelletto, X. Li and M. Gu, *Opt. Express*, 2015, **23**, 11327-11333.
32. J. Tisler, G. Balasubramanian, B. Naydenov, R. Kolesov, B. Grotz, R. Reuter, J.-P. Boudou, P. A. Curmi, M. Sennour, A. Thorel, M. Börsch, K. Aulenbacher, R. Erdmann, P. R. Hemmer, F. Jelezko and J. Wrachtrup, *ACS Nano*, 2009, **3**, 1959-1965.

33. R. Beams, D. Smith, T. W. Johnson, S.-H. Oh, L. Novotny and A. N. Vamivakas, *Nano Letters*, 2013, **13**, 3807-3811.
34. J. Stursa, J. Havlik, V. Petrakova, M. Gulka, J. Ralis, V. Zach, Z. Pulec, V. Stepan, S. A. Zargaleh, M. Ledvina, M. Nesladek, F. Treussart and P. Cigler, *Carbon*, 2016, **96**, 812-818.
35. G. Davies and M. Crossfield, *Journal of Physics C: Solid State Physics*, 1973, **6**, L104-L108.
36. M. D. Crossfield, G. Davies, A. T. Collins and E. C. Lightowlers, *Journal of Physics C: Solid State Physics*, 1974, **7**, 1909-1917.
37. S. Arroyo-Camejo, M.-P. Adam, M. Besbes, J.-P. Hugonin, V. Jacques, J.-J. Greffet, J.-F. Roch, S. W. Hell and F. Treussart, *ACS Nano*, 2013, **7**, 10912-10919.
38. N. Prabhakar, M. Peurla, S. Koho, T. Deguchi, T. Näreoja, H.-C. Chang, J. M. Rosenholm and P. E. Hänninen, 2018, **14**, 1701807.
39. S. K. Sarkar, A. Bumb, X. Wu, K. A. Sochacki, P. Kellman, M. W. Brechbiel and K. C. Neuman, *Biomedical optics express*, 2014, **5**, 1190-1202.